RESEARCH ARTICLE

Hygrothermoelastic large deflection behaviour in a thin circular plate with non-Fourier and non-Fick law

Shahala Sheikh*, Lalsingh Khalsa, Nitin Chandel, Vinod Varghese

Abstract
The coupled fractional dual phase-lag hygrothermoelasticity theory, developed using fractional calculus principles, extends classical Fourier's and Fick's laws to a time-fractional differential equation. The concept is applied to a thin circular plate that is exposed to hygrothermal loadings. The finite integral transform method and decoupled technique are utilized to create closed-form expressions for various factors such as temperature, moisture, large deflection, and stresses. The study compares the results of the dual phase-lag model with those of classical and hyperbolic models. The phase-lags parameters play a crucial role in regulating the heat and moisture transfer mechanism.

Keywords: Hygrothermoelastic, Dual-phase lag model, Circular plate, Integral transform approach, Fractional calculus, Numerical results.

Introduction

The research on thermal conduction and moisture diffusion in composites is a fascinating field involving various methods to explore the effects of heat and moisture on composite material strain and distortion. Sih and Shih (1981) used the finite difference method to analyze the influence of heat and moisture combinations on hygrothermal stresses in composite materials. Chang (1994) developed a decoupling methodology to develop analytical solutions for time-dependent stresses in both hollow and solid cylinders. Chen and Hwang (1994) utilized the finite element method to study hygrothermoelastic phenomena on a two-dimensional surface. Sobhy's (2016) plate theory provides a comprehensive understanding of the vibration and buckling characteristics of functionally graded sandwich plates. Ebrahimi and Barati (2017) utilized advanced beam theory to investigate the vibration-damping properties of viscoelastic nanobeams in hygrothermal conditions. The previously mentioned research discussed is built on the fundamental principles of the Fourier and Fick laws.

Xu *et al*. (2011) quoted that Fourier's and Fick's equations are widely utilized in classical hygrothermal systems, focusing on long-term dynamics and a wide geographical scope. Fourier's and Fick's equations may pose challenges in rapid heating and heat and moisture exchange at micro/nano-scale levels by Chester (1963), Joseph and Preziosi (1989), and Qiu and Tien (1992) in their papers. The Fourier and Fick equations suggest that heat and moisture can rapidly spread across a medium, causing uniform effects on the entire medium, as advised by Zhang *et al*. (2019). Classical Fourier and Fick equation is inefficient at micro- and nano-scale systems, leading to the development of alternative heat conduction models to better understand material heat spread. The hyperbolic heat conduction model, introduced by Cattaneo (1958) and Vernotte (1958), enhances the Fourier model by incorporating thermal relaxation, providing a more accurate representation of heat propagation's wave-like behaviour. Yang and Chen (2019) developed a precise analytical model based on non-Fourier and non-Fick concepts to describe the behavior of a half-plane with fractures exposed to sudden temperature changes. Lee *et al*. (2015) conducted a study on the non-Fourier effect in the bio-heat conduction equation, analyzing temperature and surface heat flow distributions within multiple-layered tissue. Xue *et al*. (2018) conducted a study on the impact of memory-dependent derivatives on the transient thermal stress of a fractured hollow cylinder in the hyperbolic

Department of Mathematics, M.G. College, Armori, Gadchiroli, India

*Corresponding Author: Shahala Sheikh, Department of Mathematics, M.G. College, Armori, Gadchiroli, India, E-Mail: shahalaimran@gmail.com

model. Peng *et al.* (2018) introduced the hyperbolic heat-moisture coupling model to study the dynamic behaviour of an infinite-length cylinder under hygrothermal stresses, considering its hygrothermoelastic properties. Xue *et al.* (2020) utilized the hyperbolic hygrothermal model to study the fracture problem of a cylinder with a crack along its circumference. Tzou (1995) introduced the dual-phase-lag heat conduction model (DPL model) to explain simultaneous reactions at micro and nano-scales for heat transfer. The model considers the phase-lag of heat flux and temperature gradient.

A study conducted by Tzou (1995) on delayed heat transfer in small-scale systems with fast changes found the model's superior performance in analyzing observed responses. Liu and Chen (2010) conducted a reverse study using experimental data to confirm the thermal properties of DPL in cow muscle tissue, using phase-lag values for synchronization. The DPL model's applications are not fully unstated despite studies by Zhou *et al.* (2009), Liu *et al.* (2012), Guo *et al.* (2018), Majchrzak and Mochnacki (2018), and Borjalilou *et al.* (2019), which have specifically examined the DPL heat conduction model, highlighting a gap in understanding the hygrothermal coupling model that integrates dual-phase-lag behavior and fractional calculus.

This study presents a hygrothermal coupling model incorporating a dual phase-lag effect. The objective is to analyze the transient behavior of a thin circular plate with restricted dimensions by employing fractional calculus. This analysis will consider the impact of hygrothermal loadings on the external surface. The hygrothermal distribution within a thin circular plate is estimated using integral transform techniques and a decoupling methodology. Graphical depictions of the influence of each phase-lag parameter on the hygrothermoelastic fields are operated to contrast them with the outcomes derived from classical and hyperbolic models.

Statement of the Problem

Modified dual-phase lag hygrothermoelastic theory
The microscopic approach suggested by Sih *et al.* (1986) proposed the first approximation for the variation of moisture and temperature as $M = \text{constant} + \chi C - \omega T$, where $\partial M / \partial C = \chi$ and $\partial M / \partial T = -\omega$. Then, the amount of moisture in composite per unit mass of solid, *m*, can be expressed as $\rho m = \upsilon' C + \rho M$. Due to the presence of liquid and vapor, the moisture and heat transfer obey the conservation of mass and energy as

$$\nabla \cdot q_h = \rho \gamma \frac{\partial M}{\partial t} - \rho C_p \frac{\partial T}{\partial t} \tag{1}$$

$$\nabla \cdot q_m = -\frac{\rho}{\upsilon'} \frac{\partial M}{\partial t} - \frac{\partial C}{\partial t} \tag{2}$$

Following the dual phase-lag model suggested by Peng *et al.* (2018), which incorporates delay time translation of heat

flux vector and temperature gradient, enables a microscopic examination of microstructural interactions within solid heat conductors. The proposed DPL law is found to be highly consistent with both Fourier and Fick laws:

$$\left(1 + \tau_{qh} \frac{\partial}{\partial t}\right) q_h = -k_h \left(1 + \tau_{Th} \frac{\partial}{\partial t}\right) \nabla T \tag{3}$$

$$\left(1 + \tau_{qm} \frac{\partial}{\partial t}\right) q_m = -k_m \left(1 + \tau_{Cm} \frac{\partial}{\partial t}\right) \nabla C \tag{4}$$

Eliminating variables q_h and q_m in Eqs. (1)-(4), one obtains

$$L\left(1 + \tau_{Th} \frac{\partial}{\partial t}\right) \nabla^2 T = \left(1 + \tau_{qh} \frac{\partial}{\partial t}\right)\left(\frac{\partial T}{\partial t} - \eta \frac{\partial C}{\partial t}\right) \tag{5}$$

$$D\left(1 + \tau_{Cm} \frac{\partial}{\partial t}\right) \nabla^2 C = \left(1 + \tau_{qm} \frac{\partial}{\partial t}\right)\left(\frac{\partial C}{\partial t} - \lambda \frac{\partial T}{\partial t}\right) \tag{6}$$

in which

$$L = k_h / \rho C_p \gamma \omega, \eta = \gamma \chi / C_p \gamma \omega, D = k_m \upsilon' / (\upsilon' + \rho \chi), \lambda = \rho \omega / (\upsilon' + \rho \chi) \tag{7}$$

The hygrothermoelasticity theory was reformed using the fractional derivative definition, as proposed by Caputo (1967) and Sherief *et al.* (2010), and Equations (5)-(6):

$$L\left(1 + \tau_{Th} \frac{\partial^\alpha}{\partial t^\alpha}\right) \nabla^2 T = \left(1 + \tau_{qh} \frac{\partial^\alpha}{\partial t^\alpha}\right)\left(\frac{\partial T}{\partial t} - \eta \frac{\partial C}{\partial t}\right) \tag{8}$$

$$D\left(1 + \tau_{Cm} \frac{\partial^\beta}{\partial t^\beta}\right) \nabla^2 C = \left(1 + \tau_{qm} \frac{\partial^\beta}{\partial t^\beta}\right)\left(\frac{\partial C}{\partial t} - \lambda \frac{\partial T}{\partial t}\right) \tag{9}$$

where $\partial^{(\alpha,\beta)} / \partial t^{(\alpha,\beta)}$ is understood in the sense of the Caputo time fractional derivative of $(\alpha, \beta) \in (0,1]$ of an absolutely continuous function $f(t)$ is given by

$$\frac{d^{(\alpha,\beta)}}{dt^{(\alpha,\beta)}} f(t) = I^{1-(\alpha,\beta)} \frac{d}{dt} f(t) \tag{10}$$

where I^ξ is Riemann-Liouville fractional integral of the function $f(t)$ of order ξ which is given as

$$I^\xi f(t) = \int_0^t \frac{(t-s)^{\xi-1}}{\Gamma(\xi)} f(s) ds \tag{11}$$

where $f(t)$ is a Lebesgue integrable function and $\xi > 0$.

In the context of the definition of Caputo (1967), the time-fractional derivative given by Eqs. (11) and (12), Sherief *et al.* (2010) have considered the following limiting cases:

$$\frac{d^{(\alpha,\beta)}}{dt^{(\alpha,\beta)}} f(t) = \begin{cases} f(t) - f(0), (\alpha, \beta) \to 0 \\ I^{1-(\alpha,\beta)} \frac{\partial f(t)}{\partial t}, 0 < \alpha < 1 \\ \frac{\partial f(t)}{\partial t}, (\alpha, \beta) \to 1 \end{cases} \tag{12}$$

Applying the various values of phase-lags $\tau_{qh}, \tau_{Th} \tau_{Cm}, \tau_{qm}$ and fractional order (α, β), one will obtain the following particular cases of the FDPL hygrothermal coupled model as follows:

- Taking $\tau_{qh} = \tau_{Th} = \tau_{qm} = \tau_{Cm} = 0$ and $\alpha = \beta = 1$ in Eqs. (8) and (9), then the model is parabolic and leads to the classical coupled theory suggested by Sugano and Chuuman (1993)

$$L\nabla^2 T - \partial T / \partial t + \eta_c (\partial C / \partial t) = 0,$$
$$D\nabla^2 C - \partial C / \partial t + \lambda_c (\partial T / \partial t) = 0 \tag{13}$$

- Taking $\tau_{Th} = \tau_{Cm} = 0$ and $\alpha = \beta = 1$ in lift side of Eqs. (8) and (9), then the model is hyperbolic and leads to a theory of hygrothermoelasticity suggested by Zhang and Li (2017)

$$L\nabla^2 T - [1 + \tau_{qh}(\partial^\alpha / \partial t^\alpha)](\partial T / \partial t - \eta_c \partial C / \partial t) = 0,$$
$$D\nabla^2 C - [1 + \tau_{qm}(\partial^\beta / \partial t^\beta)](\partial C / \partial t - \lambda_c \partial T / \partial t) = 0 \tag{14}$$

- Taking $\alpha = \beta$ in the above-coupled model as given in Eq. (14) with an equal fractional model suggested by Zhang and Li (2017).

Formulation of the problem

Governing equation of hygrothermal field

Let us consider a clamped circular thin plate of thickness h and radius r_0 and define it in a cylindrical system of coordinates (r, η, z). The center of the plate in the middle surface is taken as the origin, and the z-axis is normally downwards, which is subjected to heat flux and moisture flux at the surface, as shown in Figure 1.

Here, we only consider the hygrothermal effect on elastic stresses and deformation; conversely, moisture and temperature do not change due to the elastic field. We introduce the following dimensionless parameters for simplicity in analysis:

$$(\hat{r}, \hat{z}) = (r, z) / r_0, \theta = (T - T_0) / T_0, \psi = (C - C_0) / \lambda_c T_0,$$
$$(\hat{t}, \hat{t}^\alpha, \hat{\tau}_{qh}, \hat{\tau}_{Th}, \hat{\tau}_{qm}, \hat{\tau}_{Cm}) = L(t, t^\alpha, \tau_{qh}, \tau_{Th}, \tau_{qm}, \tau_{Cm}) / r_0^2, \tag{15}$$
$$\hat{w} = w / \gamma_1 T_0 r_0^2, c^2 = \beta_1^2 r_0^2, K = D / L$$

where the initial temperature and initial humidity are denoted by T_0 and C_0, respectively. With these dimensionless parameters, Eqs. (8) and (9) can be rewritten as the dimensionless expressions listed below:

$$\left(1 + \tau_{Th}\frac{\partial^\alpha}{\partial t^\alpha}\right)\nabla^2\theta = \left(1 + \tau_{qh}\frac{\partial^\alpha}{\partial t^\alpha}\right)\left(\frac{\partial\theta}{\partial t} - \eta_c\lambda_c\frac{\partial\psi}{\partial t}\right) \tag{16}$$

$$\left(1 + \tau_{Cm}\frac{\partial^\beta}{\partial t^\beta}\right)\nabla^2\psi = \left(1 + \tau_{qm}\frac{\partial^\beta}{\partial t^\beta}\right)\frac{1}{K}\left(\frac{\partial\psi}{\partial t} - \frac{\partial\theta}{\partial t}\right) \tag{17}$$

and dropping the overhat -like a symbol for simplicity and efficiency.

The linearly coupled differential equations (16) and (17) are accomplished by the following initial and physical boundary conditions with the prescribed sectional value of the matter flux, stated as

$$\theta(r,z,0) = \psi(r,z,0) = 0, \text{ for all } 0 < r < 1 \text{ and } 0 < z < \bar{h}, \tag{18}$$

$$\frac{\partial\theta(r,z,0)}{\partial t} = \frac{\partial\psi(r,z,0)}{\partial t} = 0, \text{ for all } 0 < r < 1 \text{ and } 0 < z < \bar{h}, \text{ if } \alpha, \beta > 1 \tag{19}$$
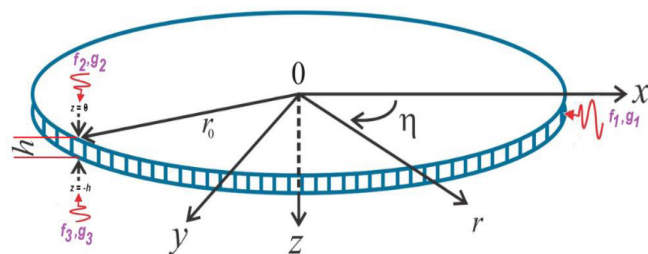

Figure 1: Schematic of a circular plate under large deflection

$$\theta(1,z,t) = f_1(z,t), \psi(1,z,t) = g_1(z,t), \text{ for all } 0 < z < \bar{h} \text{ and } t > 0, \tag{20}$$

$$\theta(r,0,t) = f_2(r,t), \psi(r,0,t) = g_2(r,t), \text{ for all } 0 < r < 1 \text{ and } t > 0, \tag{21}$$

$$\theta(r,\bar{h},t) = f_3(r,t), \psi(r,\bar{h},t) = g_3(r,t), \text{ for all } 0 < r < 1 \text{ and } t > 0, \tag{22}$$

where $f_1(z,t)$, $g_1(z,t)$, $f_2(r,t)$, $g_2(r,t)$, $f_3(r,t)$, and $g_3(r,t)$ are known.

The basic equation of large deflection formulation

If we neglect the strain energy due to the second invariant in the middle plane of the plate, then following the modified Berger approximate approach suggested by Dhakate *et al.* (2018), the equations for large deflection in dimensionless form can be given as

$$D\,\nabla^2(\nabla^2 - c^2)w = -\nabla^2 M_g(r,t) \tag{23}$$

where $D = Eh^3 / 12(1 - \upsilon^2)$ is the flexural rigidity of the plate, E is Young's modulus, υ is Poisson ratio, ∇^2 is Laplacian operator, $w = w(r,t)$ is lateral displacement, $u = u(r,t)$ is radial displacement, $M_g(r,t)$ is induced resultant moment given as

$$M_g(r,t) = \int_0^{\bar{h}} z\, g(r,z,t)\, dz \tag{24}$$

in which $g(r,z,t) = \theta + \lambda_c(\gamma_2 / \gamma_1)\psi$, and c is a normalized constant of integration in the dimensionless form given by

$$\frac{\partial u}{\partial r} + \frac{u}{r} + \frac{1}{2}\left(\frac{\partial w}{\partial r}\right)^2 = c^2 Q^2 + N_g(r,t) \tag{25}$$

with $Q^2 = \bar{h}^2(1 - \upsilon^2) / (ET_0\gamma_1 12)$, and $N_g(r,t)$ is induces resultant force:

$$N_g(r,t) = \int_0^{\bar{h}} g(r,z,t)\, dz \tag{26}$$

Consider the clamped circumference of a circular plate subjected to heat and moisture flux for which the boundary conditions:

$$w(1,t) = 0, \; \partial w(1,t) / \partial r = 0, u(1,t) = 0 \tag{27}$$

The bending stresses at the surface of the circular plate:

$$\sigma_r = \frac{6D}{h^2}\left(\frac{\partial^2}{\partial r^2} + \frac{\upsilon}{r}\frac{\partial}{\partial r}\right)w(r,t),$$
$$\sigma_\theta = \frac{6D}{h^2}\left(\upsilon\frac{\partial^2}{\partial r^2} + \frac{1}{r}\frac{\partial}{\partial r}\right)w(r,t) \tag{28}$$

Eqs. (16) to (28) constitute mathematical formulation under consideration.

Construction of the General Solution to the Problem

Solution of the hygrothermal field

Introducing Laplace transform with respect to t on both sides of fundamental Eqs. (16)-(17), with initial conditions (18)-(19). To simply further, we recall the following property of the Laplace transform of the Caputo derivative operator

$$\mathcal{L}\left\{\frac{\partial^{(\alpha,\beta)} f(t)}{\partial t^{(\alpha,\beta)}}\right\} = s^{(\alpha,\beta)} f^*(s) - \sum_{m=0}^{n-1} s^{(\alpha,\beta)-1-m}\frac{\partial^m f(0)}{\partial t^m} \tag{29}$$

where $n - 1 < (\alpha,\beta) < n$, S is the transform variable and f^* stands for the Laplace transform of f, respectively. With the help of property (29), bearing the initial boundary conditions (18)-(19) in mind, one obtains

$$(1+\tau_{Th}s^\alpha)\left(\frac{\partial^2}{\partial r^2}+\frac{1}{r}\frac{\partial}{\partial r}+\frac{\partial^2}{\partial z^2}\right)\bar\theta=(s+\tau_{qh}s^{\alpha+1})(\bar\theta-\eta_c\lambda_c\bar\psi) \quad (30)$$

$$(1+\tau_{Cm}s^\beta)\left(\frac{\partial^2}{\partial r^2}+\frac{1}{r}\frac{\partial}{\partial r}+\frac{\partial^2}{\partial z^2}\right)\bar\psi=\frac{1}{K}(s+\tau_{qm}s^{\beta+1})(\bar\psi-\bar\theta) \quad (31)$$

where overbar is the transformed function of θ and ψ.

We introduce the first-order finite Hankel integral transform of the special type to solve differential equations (30)-(31) as well as its inverse in the interval $0<r<1$ stated in Debnath and Bhatta (2007) that responds to the boundary conditions given in Eq. (20) as

$$\mathcal{H}_{1j}[f(r)]=\bar f_1(\mu_j)=\int_0^1 r\,f(r)\,J_1(r\mu_j)\,dr, j=1,2,3...,\infty \text{ discrete} \quad (32)$$

then $f(r)$ can be represented by the Fourier-Bessel series as

$$\mathcal{H}_{1j}^{-1}[\bar f_1(\mu_j)]=f(r)=2\sum_{j=1}^\infty \bar f_1(\mu_j)\frac{J_1(\mu_j r)}{J_2^2(\mu_j)}, 0<r\le 1 \quad (33)$$

and the orthogonal property as

$$\mathcal{H}_{1j}\left(\frac{d^2f}{dr^2}+\frac{1}{r}\frac{df}{dr}\right)=-\mu_j^2\,\bar f_1(\mu_j)+\mu_j J_2(\mu_j)f|_{r=1} \quad (34)$$

where the summation is taken over the positive roots of $J_1(\mu)=0$.

Further, to solve the differential equations (30)-(31), let us introduce the Fourier sine transform stated in Debnath and Bhatta (2007) in the variable z extends over a finite domain as

$$\mathcal{F}_S[g(z)]=\bar g(q)=\int_0^{\bar h} g(z)\sin(\zeta z)dz, 0\le z\le\bar h, q=1,2,3... \quad (35)$$

$$\mathcal{F}_S^{-1}[\bar g(q)]=g(z)=\frac{2}{\bar h}\sum_{q=1}^\infty \bar g(q)\sin(\zeta z), 0<z\le\bar h \quad (36)$$

From this, and the property:

$$\mathcal{F}_S\left[\frac{d^2g(z)}{dz^2}\right]=\zeta[g(0)-(-1)^q g(h)]-\zeta^2\bar g(q) \quad (37)$$

where $\sin(\zeta z)$, $\zeta=q\pi/\bar h$ is the kernel of the function.

Now, by using the integral transformation using Eq. (34), considering the condition (20); and similarly transforming the differential equations (30)-(31) using Eq. (37), bearing the boundary conditions (21)-(22) in mind the following reduction is made:

$$(1+\tau_{Th}s^\alpha)(A_1-\Omega^2\bar{\bar\theta})=s(1+\tau_{qh}s^\alpha)(\bar{\bar\theta}-\eta_c\lambda_c\bar{\bar\psi}) \quad (38)$$

$$(1+\tau_{Cm}s^\beta)(A_2-\Omega^2\bar{\bar\psi})=s(1+\tau_{qm}s^\beta)(\bar{\bar\psi}-\bar{\bar\theta})/K \quad (39)$$

where

$$\begin{aligned}&A_1=-\dot{\bar f}_2(q,s)+(-1)^n\dot{\bar{\bar f}}_3(q,s)+\bar{\bar f}_1(\mu_j)\mu_j J_1(\mu_j),\\&A_2=-\dot{\bar g}_2(q,s)+(-1)^n\dot{\bar{\bar g}}_3(q,s)+\bar{\bar g}_1(\mu_j)\mu_j J_1(\mu_j),\\&\Omega^2=\mu_j^2+\gamma^2\end{aligned} \quad (40)$$

Now, solving the Eqs. (38) and (39), one gets the dimensionless temperature and moisture in the Laplace domain below

$$\bar{\bar\theta}=\frac{(1+s^\alpha\tau_{Th})A_1 A_3-\eta_c\lambda_c s(1+s^\alpha\tau_{qh})A_2 K(1+s^\beta\tau_{Cm})}{[\Omega^2(1+s^\alpha\tau_{Th})+s(1+s^\alpha\tau_{qh})]A_3+\eta_c\lambda_c s^2(1+s^\alpha\tau_{qh})(1+s^\beta\tau_{qm})} \quad (41)$$

$$\bar{\bar\psi}=\frac{-\left\{\begin{aligned}&(1+s^\alpha\tau_{Th})s(1+s^\beta\tau_{qm})A_1+[\Omega^2(1+s^\alpha\tau_{Th})\\&+s(1+s^\alpha\tau_{qh})]A_2 K(1+s^\beta\tau_{Cm})\end{aligned}\right\}}{[\Omega^2(1+s^\alpha\tau_{Th})+s(1+s^\alpha\tau_{qh})]A_3+\eta_c\lambda_c s^2(1+s^\alpha\tau_{qh})(1+s^\beta\tau_{qm})} \quad (42)$$

where

$$A_3=-K\Omega^2(1+s^\beta\tau_{Cm})-s(1+s^\beta\tau_{qm}) \quad (43)$$

Finally, the differential equations in Eqs. (41)-(42) are solved using the inversion theorem from Eqs. (36) and (33), the solutions are found in the Laplace domain:

$$\begin{aligned}\bar\theta=\frac{4}{\bar h}\sum_{q=1}^\infty\sum_{j=1}^\infty&\frac{(1+s^\alpha\tau_{Th})A_1 A_3-\eta_c\lambda_c s(1+s^\alpha\tau_{qh})A_2 K(1+s^\beta\tau_{Cm})}{[\Omega^2(1+s^\alpha\tau_{Th})+s(1+s^\alpha\tau_{qh})]A_3+\eta_c\lambda_c s^2(1+s^\alpha\tau_{qh})(1+s^\beta\tau_{qm})}\\&\times\sin(\zeta z)J_0(\mu_j r)/J_2^2(\mu_j)\end{aligned} \quad (44)$$

$$\begin{aligned}\bar\psi=\frac{4}{\bar h}\sum_{q=1}^\infty\sum_{j=1}^\infty&\frac{-\left\langle\begin{aligned}&(1+s^\alpha\tau_{Th})s(1+s^\beta\tau_{qm})A_1+[\Omega^2(1+s^\alpha\tau_{Th})\\&+s(1+s^\alpha\tau_{qh})]A_2 K(1+s^\beta\tau_{Cm})\end{aligned}\right\rangle}{[\Omega^2(1+s^\alpha\tau_{Th})+s(1+s^\alpha\tau_{qh})]A_3+\eta_c\lambda_c s^2(1+s^\alpha\tau_{qh})(1+s^\beta\tau_{qm})}\\&\times\sin(\zeta z)J_0(\mu_j r)/J_2^2(\mu_j)\end{aligned} \quad (45)$$

The functions given in Eqs. (44) and (45) represent the temperature and moisture at every instant and all points of the circular plate of finite height in the Laplace domain.

Now, substituting Eqs. (44) and (45) into $g(r,z,t)=\theta+\lambda_c(\gamma_2/\gamma_1)\psi$, one obtains

$$\bar g(r,z,s)=\frac{4}{\bar h}\sum_{q=1}^\infty\sum_{j=1}^\infty\frac{\phi(s)J_0(\mu_j r)}{J_2^2(\mu_j)}\sin(\zeta z) \quad (46)$$

where

$$\phi(s)=\frac{\left\langle\begin{aligned}&(1+s^\alpha\tau_{Th})\{A_1 A_3-\lambda_c(\gamma_2/\gamma_1)[s(1+s^\beta\tau_{qm})A_1+\Omega^2 A_2 K\\&(1+s^\beta\tau_{Cm})]\}-s(1+s^\alpha\tau_{qh})A_2 K(1+s^\beta\tau_{Cm})\lambda_c[\eta_c+(\gamma_2/\gamma_1)]\end{aligned}\right\rangle}{[\Omega^2(1+s^\alpha\tau_{Th})+s(1+s^\alpha\tau_{qh})]A_3+\eta_c\lambda_c s^2(1+s^\alpha\tau_{qh})(1+s^\beta\tau_{qm})} \quad (47)$$

Solution of the large deflection

Substituting Eq. (46) into transformed Eq. (24) and (26), one obtains

$$M_g(r,s)=\frac{4}{\bar h}\sum_{q=1}^\infty\sum_{j=1}^\infty\frac{\phi(s)\nu_1 J_0(\mu_j r)}{\zeta^2 J_2^2(\mu_j)} \quad (48)$$

$$N_g(r,s)=\frac{4}{\bar h}\sum_{q=1}^\infty\sum_{j=1}^\infty\frac{\phi(s)\nu_2 J_0(\mu_j r)}{\zeta J_2^2(\mu_j)} \quad (49)$$

where $\nu_1=\sin(\zeta\bar h)-\zeta\bar h\cos(\zeta\bar h)$ and $\nu_2=1-\cos(\zeta\bar h)$.

Now substituting Eq. (48) into transformed Eq. (23), one obtains

$$\nabla^2(\nabla^2-c^2)w(r,s)=\frac{4}{\bar hD}\sum_{q=1}^\infty\sum_{j=1}^\infty\frac{\phi(s)\nu_1\mu_j^2 J_0(\mu_j r)}{\zeta^2 J_2^2(\mu_j)} \quad (50)$$

We assume $w(r,s)$ that it satisfies boundary conditions (27) and Eq. (50):

$$w(r,s) = \frac{4}{\bar{h}D} \sum_{q=1}^{\infty} \sum_{j=1}^{\infty} \frac{\mu_j{}^2 v_1 \phi(s)[J_0(\mu_j r) - J_0(\mu_j)]}{\zeta^2 J_2^2(\mu_j)[\mu_j{}^2(\mu_j{}^2 + c^2)]} \tag{51}$$

Substituting Eqs. (49) and (51) into (52). and integrating with respect to r, one gets

$$u = \frac{rc^2 Q^2}{2} + \frac{4}{\bar{h}r} \sum_{q=1}^{\infty} \sum_{j=1}^{\infty} \frac{\phi(s)}{J_2^2(\mu_j)} \left\langle rJ_1(\mu_j r) v_2 / \zeta \right.$$

$$- \frac{\phi(s)}{J_2^2(\mu_j)} \frac{1}{D} \left[\frac{-\mu_j}{\zeta^2[\mu_j{}^2(\mu_j{}^2 + c^2)]} \right]^2 v_1^2 \tag{52}$$

$$\times \left\{ \mu_j{}^2 r^2 [J_1'(\mu_j r)]^2 + (\mu_j{}^2 r^2 - 1)[J_1(\mu_j r)]^2 \right\} \right\rangle + C_1$$

where $J_1'(\mu_j r) = [J_0(\mu_j r) - J_2(\mu_j r)]/2$.

Using boundary condition (27) and Eq. (52), one obtains

$$C_1 = -\frac{c^2 Q^2}{2} + \frac{4}{\bar{h}} \sum_{q=1}^{\infty} \sum_{j=1}^{\infty} \frac{1}{D} \left[\frac{\mu_j{}^2 v_1{}^2 \phi(s) J_1'(\mu_j)}{\zeta^2[\mu_j{}^2(\mu_j{}^2 + c^2)]J_2^2(\mu_j)} \right]^2 \tag{53}$$

Substituting Eqs. (34)-(36) into Eq. (9), one obtains

$$\sigma_r = -\frac{24}{\bar{h}^3} \sum_{q=1}^{\infty} \sum_{j=1}^{\infty} \frac{\mu_j v_1 \phi(s)}{\zeta^2 J_2^2(\mu_j)(\mu_j{}^2 + c^2)} \left[\mu_j J_0(\mu_j r) - \frac{(1-\upsilon)}{r} J_1(\mu_j r) \right] \tag{54}$$

$$\sigma_\theta = -\frac{24}{\bar{h}^3} \sum_{q=1}^{\infty} \sum_{j=1}^{\infty} \frac{v_1 \mu_j \phi(s)}{\zeta^2 J_2^2(\mu_j)(\mu_j{}^2 + c^2)} \left[\upsilon \mu_j J_0(\mu_j r) - \frac{(1-\upsilon)}{r} J_1(\mu_j r) \right] \tag{55}$$

and at stress at $r = 1$ can be obtained as

$$(\sigma_r)_{r=1} = -\frac{24}{\bar{h}^3} \sum_{q=1}^{\infty} \sum_{j=1}^{\infty} \frac{\mu_j v_1 \phi(s) \mu_j J_0(\mu_j)}{\zeta^2 J_2^2(\mu_j)(\mu_j{}^2 + c^2)} \tag{56}$$

$$(\sigma_\theta)_{r=1} = -\frac{24}{\bar{h}^3} \sum_{q=1}^{\infty} \sum_{j=1}^{\infty} \frac{\upsilon v_1 \mu_j \phi(s) \mu_j J_0(\mu_j)}{\zeta^2 J_2^2(\mu_j)(\mu_j{}^2 + c^2)} \tag{57}$$

Eqs. (56) and (57) give a relationship as

$$(\sigma_\theta)_{r=1} = \upsilon (\sigma_r)_{r=1} \tag{58}$$

The Numerical Inversion of the Laplace Transforms

Applying the Gaver-Stehfest algorithm suggested by Stehfest (1970) to obtain the inverse Laplace transform to approximate the time domain solution as

$$f(t) \approx f_M(t) = \frac{\ln(2)}{t} \sum_{k=1}^{2M} a_\ell \bar{f} \left[\frac{k \ln(2)}{t} \right],$$

$$a_\ell = (-1)^{M+k} \left[\sum_{\ell=(k+1)/2}^{\ell=\min(k,M)} \frac{\ell^{M+1}}{M!} \binom{M}{\ell}\binom{2\ell}{\ell}\binom{\ell}{k-\ell} \right], \tag{59}$$

where $n \geq 1$, $t > 0$, $1 \leq M \leq \ell$, $\bar{f}$ is the Laplace transform of $f(t)$, $2M$ is an even integer whose value depends on the word length of the computer used. Kuznetsov (2013) has established the convergence of the Gaver-Stehfest algorithm for the numerical inversion of the Laplace transform.

Numerical Results, Discussion, and Remarks

This section focuses on numerically calculating the large deflection of a circular plate made of a composite material. The analysis takes into account the hygrothermoelastic behavior of the material, considering its specific material

properties: $E = 64.3$ GPa, $\eta = 0.5$ cm^3 °C/g, $D = 2.16 \times 10^{-6}$ m^2/s, $\Lambda = 2.16 \times 10^{-5}$ m^2/s, $v = 0.33$, $\rho = 1590$ kg/m^3, $\lambda = 0.5$ g/(cm^3 °C), $\gamma_1 = 31.3 \times 10^{-6}$ cm/(cm °C), $\gamma_2 = 2.68 \times 10^{-3}$ cm/(cm%H$_2$O) as inscribed in Sih and Shih (1981). The study uses numerical simulations to investigate the impact of hygrothermoelastic response on a thin plate, highlighting the need for further research using the Berger approximation hypothesis. The analysis focuses on a circular plate exposed to constant hygrothermal loading on the top edge, maintaining zero temperature for the curved circular surface and lower edge. The MATHEMATICA software generated figures presenting the variation of temperature, moisture, large deflection, radial stress, and circumferential stress distribution along r and z for different periods. The solid line represents the coupled hygrothermoelastic distribution, while the dotted line represents the uncoupled model.

Figure 2 shows a dimensionless temperature distribution along r, indicating that the temperature distribution grows linearly from zero to positive values for various r values. It shows that the sectional heat supply may be responsible for temperature changes. At the curved surface of the circular plate, this heat supply produces tensile tension and a greater temperature magnitude. If the temperature is zero, the
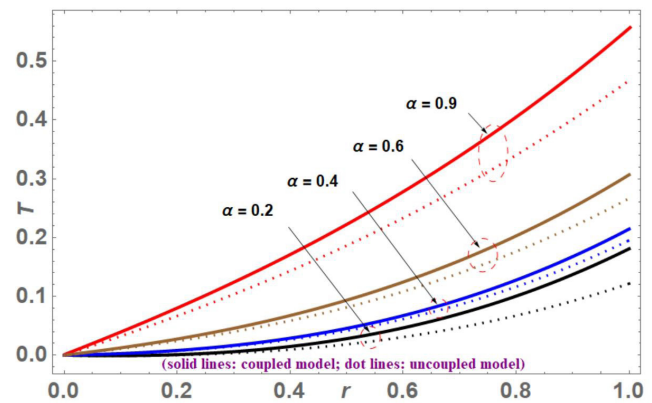

Figure 2: Temperature distribution along r at various α`

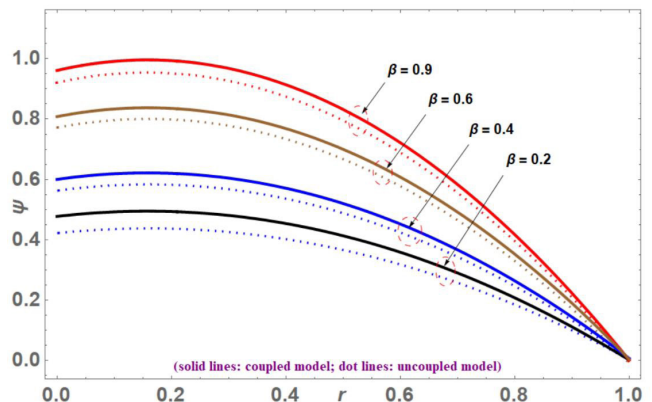**Figure 3:** Moisture distribution along r at various β

boundary condition is met, and the maximal compressive force operates at the plate's origin. Figure 3 shows the dimensionless moisture distribution along the r-axis of a circular plate. The temperature distribution shows a linear drop from positive values to zero for different r values. This decrease in moisture content is due to the moisture being initially at the center of the plate. The sectional heat supply is directed towards the plate's curved surface, causing a greater moisture force at the plate's origin. The plate experiences the most compressive stress along its curved surface, resulting in zero moisture content and meeting boundary requirements.

Figure 4 depicts the transverse deflection of a clamped circular plate seen across different fractional orders $\alpha = 0.2, 0.4, 0.6, 0.9$. The large deflection was found to be most significant near the center of the plate. When the value of r becomes unity, the distribution of deflection gradually decreases as we approach the outer circular boundary surface of the plate. The observation reveals that the radial stress function is compressive in nature at the origin, as seen in Figure 5. The findings of the investigation indicate a direct proportionality between the radial stress and the fractional order α in the radial direction. The radial stress exhibits an immediate rise within the range $0 < r < 0.2$

as a result of the substantial tensile force, followed by a gradual increase after that. The compressive force exhibits its highest magnitude at the outer circular boundary surface of the thin plate at a point $r = 1$. Similar patterns may be detected in the distribution of circumferential stress along the r-axis, as shown in Figure 6. The fluctuation in temperature during dimensionless time t is seen in Figure 7, showcasing different fractional order parameter values α. It has been shown that the temperature distribution exhibits an initial increase with positive values for $0 < t < 1$, followed by a subsequent decrease until $1 < t < 3.5$. Subsequently, a modest stabilization is seen from $t > 3.5$ for all phase-lags being examined.

The moisture distribution ψ exhibits that initial moisture decreases when $0 < t < 0.05$, followed by a progressive rise from $0.05 < t < 0.2$, and reaches stability at $t > 0.2$ for all phase-lags and fractional order values examined, as seen in Figure 8. According to Figure 9, the deflection distribution tends towards zero at $t = 0$ and $t > 0.2$ as a result of the initial exertion of a stronger compressive force. Conversely, the temperature reaches its greatest value at $t = 0.05$ owing to the influence of the tensile force. Hence, the curves have a somewhat bell-shaped deflection distribution. Figure 10 illustrates the trajectory of the radial stress curve,
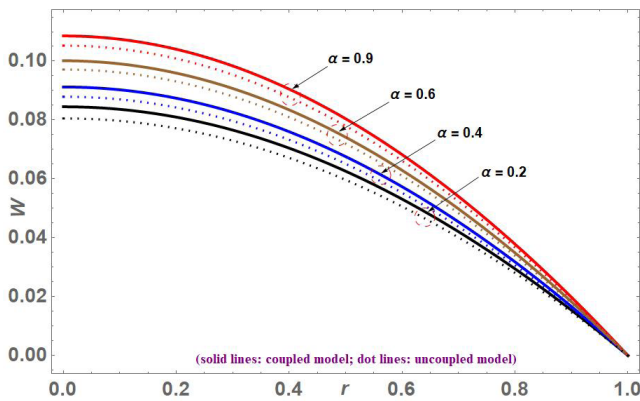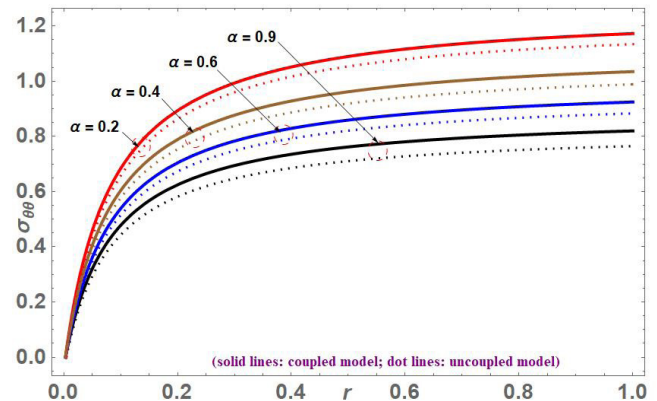

Figure 4: Deflection profile along r at various α

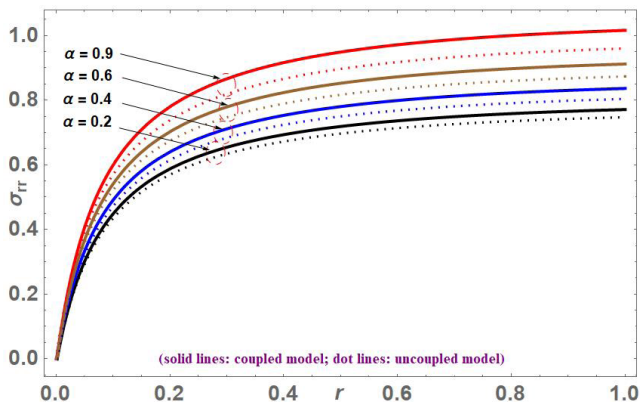**Figure 6:** Circumferential stress distribution along r at various α

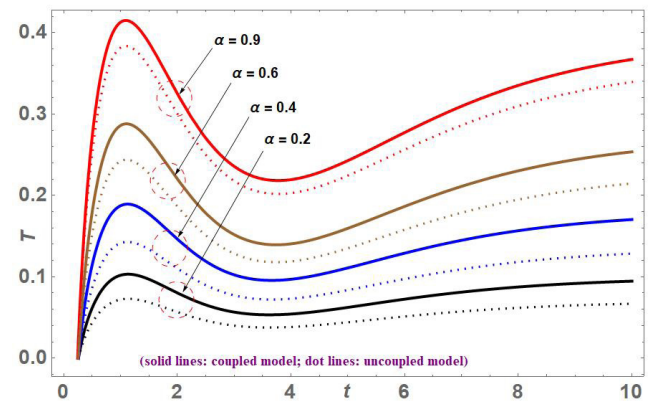**Figure 5:** Radial stress distribution along r at various α

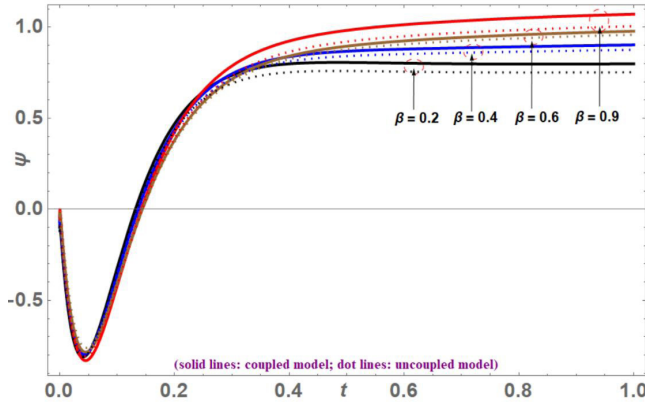**Figure 7:** Temperature distribution along t at various α

Figure 8: Moisture distribution along t at various β

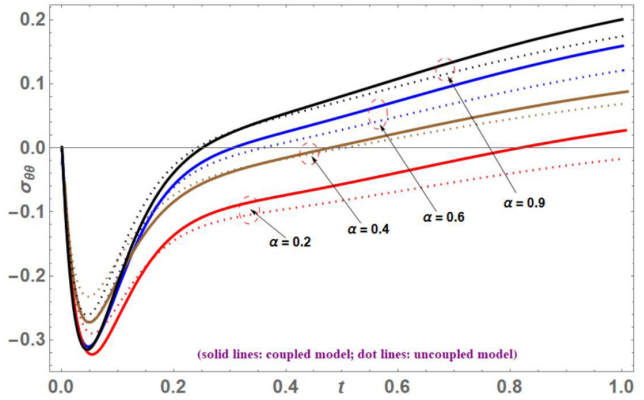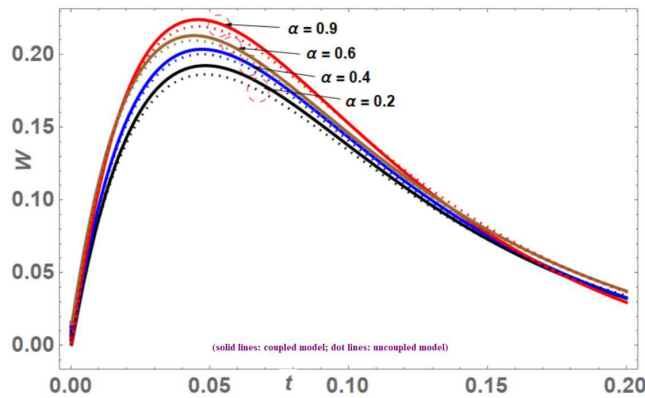**Figure 11:** Circumferential stress distribution along t at various α

Figure 9: Deflection distribution along t at various α

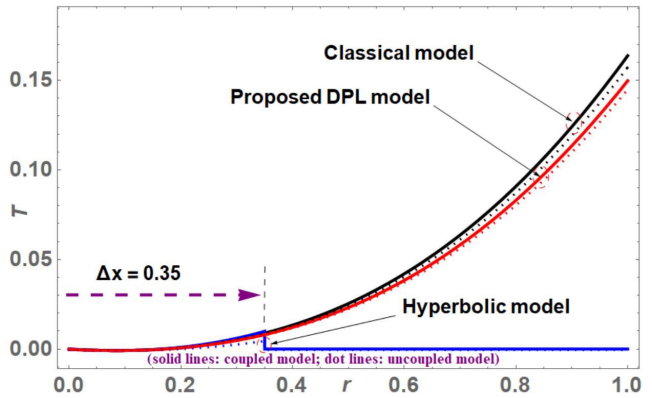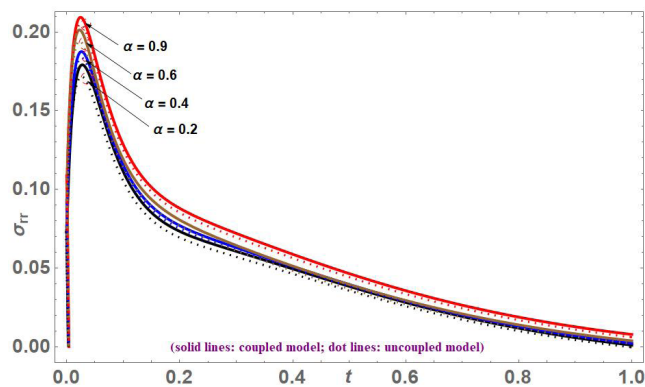**Figure 12:** Comparisons between the two models with α = 0.3

Figure 10: Radial stress profile along t at various α

The current model goes through a comparative analysis with various models in order to evaluate its reliability, as illustrated in Figure 12. Following Gao and Ma (2021), it is learned that the propagation distance $\Delta x = Vt = \{50\}^{1/2} t = 0.35$ (here $t = 0.05$), is in good agreement with the numerical prediction, as shown in Figure 12. The integral across a region represents the heat absorbed from an external heat source, whereas the temperature distributions of distinct models show alternative heat transfer mechanisms occurring at a particular moment.

Conclusion

The proposed study examines a hygrothermoelastic problem involving coupled fractional dual-phase-lag transient heat and moisture diffusion that obeys non-Fourier and non-Fick's laws. The thin circular plate is subjected to physical hygrothermal load at its outer surface. An integral transform technique was employed to derive closed-form solutions for the hygrothermal distribution, and its impact on large deflection is studied. Specifically, outcomes are related to those obtained from parabolic and hyperbolic hygrothermal models, which were considered an exact case of the current model. Graphic illustrations have been

which first exhibits an upward trend until reaching its peak. Subsequently, it undergoes an exponential decline, ultimately aligning with time *t*. The circumferential stress exhibits a decrease to a minimum when the value of time ranges from $0 < t < 0.05$, followed by a progressive rise from $t > 0.05$, and eventually reaches stability at $t > 0.2$ for all fractional order parameter values *a*, for all phase-lags being examined, as seen in Figure 11.

generated to depict the numerical outcomes relevant to the transient hygrothermoelastic phenomena. The numerical results yield several inferences:

- The associated non-Fourier and non-Fick effects under fractional order and phase-lags significantly affect the response history and propagation of hygrothermal fields, mostly due to a non-Fourier effect. Even in the absence of heat transmission to the surroundings, energy dissipation may result in a drop in temperature.

- Following the theoretical framework of hygrothermoelasticity with one-temperatures, it is necessary to establish a revised categorization system for materials based on their phase lag for evaluating the materials' capacity to facilitate the conduction of heat and moisture while considering the influence of hygrothermoelastic properties.

- The theories of coupled classical hygrothermoelasticity, generalized hygrothermoelasticity with two relaxation times, and Caputo time fractional derivatives can be derived as specific instances.

This research enhances the design of machines or structures in engineering contexts by incorporating suitable factors and functions into expressions.

Nomenclature

T	temperature	q_m	moisture flux vector
∇^2	Laplace operator	q_h	heat flux vector
χ, ω	material constants	γ	heat released from a unit mass
C	mass of moisture	c_p	specific heat
υ'	volume fraction of the voids	k_h	thermal conductivity
ρ	density of the material	k_m	moisture diffusion coefficient
∇	gradient operator	τ_{qh}	relaxation time of heat flux
u	radial displacement	τ_{qm}	relaxation time of moisture
σ_r	radial stress	τ_{Th}	phase-lag of heat gradient
σ_θ	tangential stress	τ_{Cm}	phase-lag of moisture gradient
ψ	moisture distribution	γ_1	thermal expansion coefficient
υ	Poisson ratio	γ_2	moisture expansion coefficient
α, β	fractional order	s	transformed parameter

Acknowledgment

Contribution Author's

All authors shared with the same percentage

References

Borjalilou, V., Asghari, M., and Bagheri, E. (2019). Small-scale thermoelastic damping in microbeams utilizing the modified couple stress theory and the dual-phase-lag heat conduction model, J. Therm. Stress., Vol. 5, No. 3, pp. 1-14. DOI: 10.1080/01495739.2019.1590168

Cattaneo, C. (1958). A form of heat conduction equation which eliminates the paradox of instantaneous propagation, Comp. Rend., Vol. 247, No. 4, pp. 431-433.

Chester, M. (1963). Second sound in solids, Phys. Rev., Vol. 131, pp. 2013-2015. DOI:10.1103/PhysRev.131.2013

Caputo, M. (1967). Linear models of dissipation whose Q is almost frequency independent-II, Geophys. J. Int., Vol. 13, No. 5, pp. 529-539. DOI: 10.1111/j.1365-246X.1967.tb02303.x

Chang, W. J. (1994). Transient hygrothermal responses in a solid cylinder by linear theory of coupled heat and moisture, Appl. Math. model., Vol. 18, No. 8, pp. 467-473. DOI: 10.1016/0307-904X(94)90309-3

Chen, T. C. and Hwang, B. H. (1994). Transient hygrothermal stresses induced in two-dimensional problems by nonlinear theory of coupled heat and moisture, J. Appl. Mech. Trans. ASME, Vol. 61, No. 4, pp. 938-943. DOI: 10.1115/1.2901582

Debnath, L. and Bhatta, D.(2007). Integral transforms and their applications, 2nd Edition, C.R.C. Press, London

Dhakate, T., Varghese, V., and Khalsa, L. (2018). A simplified approach for the thermoelastic large deflection in the thin clamped annular sector plate, J. Therm. Stress., Vol. 42, No. 3, pp. 271- 285. DOI: 10.1080/01495739.2017.1361369

Ebrahimi, F. and Barati, M. R. (2017). Hygrothermal effects on vibration characteristics of viscoelastic FG nanobeams based on nonlocal strain gradient theory, Compos. Struct., Vol.159, pp. 433-444. DOI: 10.1016/j.compstruct.2016.09.092

Guo, S. L., Wang, B. L., and Li, J. E. (2018). Surface thermal shock fracture and thermal crack growth behavior of thin plates based on dual-phase-lag heat conduction, Theor. Appl. Fract. Mech., Vol. 96, pp. 105-113. DOI: 10.1016/j.tafmec.2018.04.007

Gao, Y. and Ma, Y. (2021). Dynamic response of a hollow cylinder under memory-dependent differential hygrothermal coupling, J. Therm. Stress, Vol. 44, No. 12, pp. 1441-1457. DOI: 10.1080/01495739.2021.1993763

Joseph, D. D. and Preziosi, L. (1989). Heat waves, Rev. Mod. Phys., Vol. 61, pp. 41-73. DOI: 10.1103/RevModPhys.61.41

Kuznetsov, A. (2013). On the convergence of the GaverâĂˇ Sˏ Stehfest algorithm, SIAM J. Num. Anal., Vol. 51, No. 6, pp. 2984-2998. DOI: 10.1137/13091974X

Liu, K. C. and Chen, H. T. (2010). Investigation for the dual phase lag behavior of bio-heat transfer, Int. J. Therm. Sci., Vol. 49, No. 7, pp. 1138-1146. DOI:10.1016/j.ijthermalsci.2010.02.007

Liu, K. C., Wang, Y. N., and Chen, Y. S. (2012). Investigation on the bio-heat trans- fer with the dual-phase-lag effect, Int. J. Therm. Sci., Vol. 58, pp. 29-35. DOI: 10.1016/j.ijthermalsci.2012.02.026

Lee, H. L. Chen, W. L. Chang, W. J., and Yang, Y. C. (2015). Estimation of surface heat flux and temperature distributions in a multilayer tissue based on the hyperbolic model of heat conduction, Comput. Methods Biomech. Biomed. Eng., Vol. 18, No. 14, pp. 1525-1534. DOI: 10.1080/10255842.2014.925108

Majchrzak, E. and Mochnacki, B. (2018). Dual-phase lag model of thermal processes in a multi- layered microdomain subjected to a strong laser pulse using the implicit scheme of FDM, Int. J. Therm. Sci., Vol. 133, pp. 240-251. DOI: 10.1016/j.

ijthermalsci.2018.07.030

Peng, Y., Zhang, X. Y., Xie, Y. J., and Li, X. F.(2018). Transient hygrothermoelastic response in a cylinder considering non-Fourier hyperbolic heat-moisture coupling, Int. J. Heat Mass Transf., Vol. 126, pp. 1094-1103. DOI: 10.1016/j.ijheatmasstransfer.2018.05.084

Qiu, T. Q. and Tien, C. L. (1992). Short-pulse laser heating on metals, Int. J. Heat Mass Transf., Vol. 35, No. 3, pp. 719-726. DOI: 10.1016/0017-9310(92)90131-B

Sih, G. C. and Shih, M. T. (1980). Transient hygrothermal stresses in composites: coupling of moisture and heat with temperature varying diffusivity, Int. J. Eng. Sci., Vol. 18, No. 1, pp. 19-42. DOI: 10.1016/0020-7225(80)90004-X

Sih, G. C. Michopoulos, J. and Chou, S. C.(1986). Hygrothermoelasticity, Martinus Niijhoof Publishing, Dordrecht

Stehfest, H. (1970). Algorithm 368, Numerical inversion of Laplace transforms, Comm. Assn. Comp. Mach., Vol. 13, No. 1, pp. 47-49. DOI:10.1145/361953.361969

Sugano, Y. and Chuuman, Y. (1993). Analytic solution of transient hygrothermoelastic problem due to coupled heat and moisture diffusion in a hollow circular cylinder, Trans. Jpn Soc. Mech. Eng., Vol. 59, No. 564, pp. 1956-1963.

Sherief, H. H., El-Sayed, A. M. A., and Abd El-Latief, A. M. (2010). Fractional order theory of thermoelasticity, Int. J. Solids Struct., Vol. 47, No. 2, pp. 269-275. DOI: 10.1016/j.ijsolstr.2009.09.034

Sobhy, M. (2016). An accurate shear deformation theory for vibration and buckling of FGM sandwich plates in hygrothermal environment, Int. J. Mech. Sci., Vol. 110, pp. 62-77. DOI: 10.1016/j.ijmecsci.2016.03.003

Tzou, D. Y. (1995). A unified field approach for heat conduction from macro-to micro-scales, J. Heat Transf. Trans. ASME, Vol. 117, No. 1, pp. 8-16. DOI: 10.1115/1.2822329

Tzou, D. Y. (1995). Experimental support for the lagging behavior in heat propagation, J. Thermo- phys. Heat Transf., Vol. 9, No. 4, pp. 686-693. DOI: 10.2514/3.725

Vernotte, P. (1958). Paradoxes in the continuous theory of the heat conduction, Comp. Rend., Vol. 246, pp. 3154-3155. DOI: 10.1016/j.ijengsci.2017.06.006

Xu, M. T., Guo, J. F., Wang, L. Q. and Cheng, L. (2011). Thermal wave interference as the origin of the overshooting phenomenon in dual-phase-lagging heat conduction, Int. J. Therm. Sci., Vol. 50, pp. 825-830. DOI: 10.1016/j.ijthermalsci.2010.12.006

Xue, Z. N., Chen, Z. T., and Tian, X. G. (2018). Transient thermal stress analysis for a circumferentially cracked hollow cylinder based on memory-dependent heat conduction model, Theor. Appl. Fract. Mech., Vol. 96, pp. 123-133. DOI: 10.1016/j.tafmec.2018.04.008

Xue, Z. N., Tian, X. G., and Liu, J. L. (2020). Non-classical hygrothermal fracture behavior of a hollow cylinder with a circumferential crack, Eng. Fract. Mech., Vol. 224, pp. 106805. DOI: 10.1016/j.engfracmech.2019.106805

Yang, W. Z. and Chen, Z. T. (2019). Investigation of the thermal-elastic problem in cracked semi-infinite FGM under thermal shock using hyperbolic heat conduction theory, J. Therm. Stress., Vol. 42, No. 8, pp. 993-1010. DOI: 10.1080/01495739.2019.1590170

Zhou, J. H., Zhang, Y. W., and Chen, J. K.(2009). An axisymmetric dual-phase-lag bioheat model for laser heating of living tissues, Int. J. Therm. Sci., Vol. 48, No. 8, pp.1477-1485. DOI: 10.1016/j.ijthermalsci.2008.12.012

Zhang, X. Y. and Li, X. F.(2017). Transient response of a hygrothermoelastic cylinder based on fractional diffusion wave theory, J. Therm. Stress., Vol. 40, pp.1575-1594. DOI:10.1080/01495739.2017.1344111

Zhang, X. Y., Peng, Y. Xie, Y. J., and Li, X. F. (2019). Hygrothermoelastic response of a hollow cylinder based on a coupled time-fractional heat and moisture transfer model, Z. Angew. Math. Phys., Vol. 70, No. 2, pp. 1-21. DOI: 10.1007/s00033-018-1047-1